







Optimization of a Thermal Ice Protection System by Means of a Genetic Algorithm

Bárbara Arizmendi Gutiérrez^(✉) , Alberto Della Noce ,
Mariachiara Gallia , and Alberto Guardone 

Politecnico di Milano, Via Giuseppe La Masa, 34, 20156 Milano, Italy
barbara.arizmendi@polimi.it

Abstract. Ice accretion poses a major threat for performance and safety of aircraft. Electro-Thermal Ice Protection Systems (ETIPS) are a reliable and flexible alternative to protect critical parts against it. Their main drawback is the high power consumption, especially when operating in fully evaporative Anti-Ice mode. In this work, a Genetic Algorithm (GA) is deployed to optimize the heat flux distribution on the fixed heaters of a wing ETIPS that operates in Anti-Ice regime. The aim is to minimize the power consumption while ensuring safety, such that no runback ice is formed downstream the protected parts. A thermodynamic numerical model was deployed to assess runback ice formations for each layout of heat fluxes. A linear penalty method was selected to handle the constraint of no-runback ice formation. Crossover and Mutation operators for GA were investigated for a large population as well as a penalty factor. Higher penalties and Mutation-based GA presented the best optimization performance based on several runs. The optimal layout of fluxes was found to minimize as well the convective losses in several ways to increase the evaporative efficiency.

Keywords: In-flight icing · Ice Protection Systems · Optimization · Genetic Algorithms

Nomenclature

Parameters

Δl_i	Size of the heater i [m]	H	IPS Substratum thickness [m]
δ	Thickness [m]	h	Heat Transfer Coefficient [$\text{Wm}^{-2}\text{K}^{-1}$]
\dot{m}	Mass Rate [kgs^{-1}]	i_{l-s}	Solidification latent heat [Jkg^{-1}]
\dot{Q}	Thermal Power [Wm^{-1}]	i_{l-v}	Vaporization latent heat [Jkg^{-1}]
\dot{q}''	Heat Flux [Wm^{-2}]	k_{wall}	Effective Thermal Conductivity
\mathbf{P}	Heat Fluxes vector	l	Number of chromosome gens
A	Control volume surface area [m^2]	p	Probability
		P_i	Heat Flux of the heater i [Wm^{-2}]

c	Chord [m]	s	Curvilinear Coordinate [m]
c_p	Specific Heat [$\text{Jkg}^{-1}\text{K}^{-1}$]	T	Temperature [K]
F	Wetness fraction	V	Velocity [ms^{-1}]
LWC	Liquid Water Content [kgm^{-3}]	imp	Impinging
MVD	Mean Volume Diameter [μm]	in	Incoming to a control volume
Subscripts		IPS	Ice protection system
0	Total	m	Mutation
∞	Free stream	out	Outgoing from a control volume
A	Average of runs	rec	Recovery
B	Best of all runs	ref	Reference Temperature, 273.15K
cr	Crossover	$wall$	External solid surface
f	Liquid film	$water$	Liquid film
ice	Freezing		

1 Introduction

Aircraft icing consists of the accumulation of ice on their surfaces when interacting with supercooled clouds. These contain water droplets that are at a temperature below the freezing point but they remain liquid in metastable equilibrium. When the droplets impact, they totally or partially freeze [9]. Among other effects, in-flight icing causes a reduction in the lift capability, increase in drag, decrease of the control surface effectiveness [10]. Furthermore, severe ice accretions have been the cause of several accidents in the past [14]. According to literature, “the average altitude of icing environments is around 3 000 m above mean sea level, with few encounters above 6 000 m” [15]. Commonly, aircraft operate at these altitudes and for this reason, the critical parts of aircraft must include Ice Protection Systems (IPS). Anti-Ice operational regime of IPS prevents the formation of ice and it includes two operating modes: fully evaporative and running wet. Electro-Thermal IPS (ETIPS) is a mature technology widely deployed to protect small critical parts due to its reliability. It consists of a substratum including resistors to transform electricity into heating power. One of its main drawbacks a high power consumption compared to other technologies, especially in fully evaporative operation for large protected areas in long icing encounters. Also, when operating in running wet regime, the water that is not evaporated might freeze downstream forming the so-called runback ice. Runback ice also compromises safety and performance. Wing ETIPS are deployed in several substratum heating bands that extend spanwise and can be controlled independently. Despite its drawbacks, there is room for improvement and motivation for such in the development of fully electric aircraft.

There is a very limited research effort available in open literature concerning ETIPS experimental studies, mainly due to high cost and confidentiality. A study conducted by Al-Khalil [1] consists of a set of icing wind tunnel tests of an ETIPS. However, there is a large research effort on the development of

numerical models for the prediction of the performance of Thermal Anti-Ice ETIPS. Numerical models aim to support preliminary designs and to improve the understanding of the physics. These codes include ANTICE [1], FENSAP-ICE [2], the works by Silva [18,19] and many others. They are based on the formulation of mass and energy conservation equations in control volumes. With the development of numerical codes, there is a recent research effort on optimizing their power consumption. Pellisier [13] performed a surrogate-based numerical optimization study of the geometric parameters of Pneumatic wing IPS. The goal was to minimize the power consumption while ensuring all water was evaporated employing GA. Pourbagian performed a surrogate-based optimization study of a wing Anti-Ice ETIPS in both operational modes [16] utilizing Multi-Adaptive Direct Search. Further work of Pourbagian [17] included several formulations of objective functions and constraints for the optimization of an Anti-Ice ETIPS.

In this work, the minimization of the thermal power consumption of an Anti-Ice ETIPS working in fully evaporative regime was performed utilizing a GA. Several Genetic operators were investigated and compared to find the best performing one. The numerical framework of optimization of the IPS includes only in-house developed and open-source codes. It is aimed to obtain an understanding of the physics of optimized configurations compared to intuitive designs, hence the identification of the global minimum is only advantageous. In Sect. 2, the framework for numerical simulations is presented. Section 3 describes the optimization methodology including the objective function selected. In Sect. 4, the results obtained are presented and discussed. Finally in Sect. 5 the concluding remarks are explained.

2 Numerical Modelling

2.1 Model Equations

Several assumptions and simplifications were introduced to enable the model construction. Steady-state was assumed, given that generally, Anti-Ice systems deal with long exposures to icing conditions. The physical process was decomposed in several loosely coupled numerical steps. The discretization of the computational domain was performed utilizing the in-house software uhMesh [7]. The computation of the Aerodynamic field was performed through the CFD code SU2 [8]. The flow was modelled as inviscid and the resulting velocity field for the reference test case is presented in Fig. 1. The distribution of water impingement was computed by means of the in-house software PoliDrop [3]. It consists of a Lagrangian Particle Tracking solver that computes the trajectories of water droplets in an aerodynamic field. The distribution of water on the surface is quantified by the collection efficiency. The obtained profile for the reference test case is presented in Fig. 2. The thermal calculations were performed by the Anti-Ice module of PoliMice. It solved mass and energy conservation equations. The model equations were based on the work of Silva [18,19] while the liquid film model is based on the work of Myers [12] adapted to the Anti-Ice problem. The equations are

solved in a discrete domain divided into control volumes. The mass conservation equation reads:

$$\frac{\partial \delta_f \bar{u}_f (\delta_f, s)}{\partial s} = \frac{\dot{m}_{imp} - \dot{m}_{evap} - \dot{m}_{ice}}{A \rho_{H_2O}} \quad (1)$$

From δ_f , \dot{m}_{in} and \dot{m}_{out} can be retrieved. The equation of the energy conservation in the solid substratum of the IPS is presented next:

$$\begin{aligned} \frac{d}{ds} (k_{wall} H \frac{dT_{wall}}{ds}) - F h_{water} (T_{wall} - T_{water}) + \dot{q}''_{IPS} \\ - (1 - F) [h_{air} (T_{wall} - T_{rec})] = 0 \end{aligned} \quad (2)$$

Finally, a second conservation equation in the liquid film is formulated:

$$\begin{aligned} F A h_{air} (T_{rec} - T_{water}) + F A h_{water} (T_{wall} - T_{water}) \\ + \dot{m}_{in} c_{p_{water}} (T_{in} - T_{ref}) - \dot{m}_{out} c_{p_{water}} (T_{out} - T_{ref}) \\ + \dot{m}_{imp} \left[c_{p_{water}} (T_{\infty} - T_{ref}) + \frac{V_{\infty}^2}{2} \right] \\ - \dot{m}_e [i_{l-v} + c_{p_{water}} (T_{water} - T_{ref})] \\ + \dot{m}_{ice} [i_{l-s} - c_{p_{water}} (T_{water} - T_{ref})] = 0. \end{aligned} \quad (3)$$

The main heat fluxes in Eq. 3 are the evaporative and convective ones. The convective heat fluxes are inefficiencies as ideally all the thermal power supplied would be devoted to evaporation. The evaporative heat flux depends exponentially on the temperature whereas the convective heat flux is linear. It is assumed there is no temperature gradient across the height of the film. Terms to predict

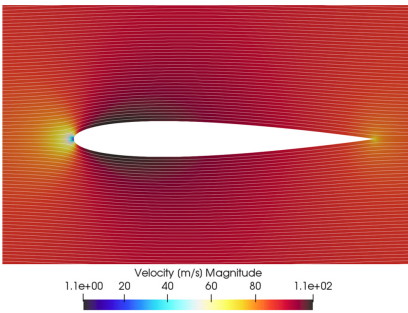


Fig. 1. Airflow velocity field computed by means of the CFD software SU2 for the test case 67A

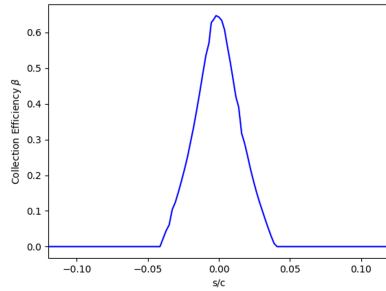


Fig. 2. Water collection efficiency computed by means of PoliDrop. The 0 abscissa corresponds to the leading edge of the airfoil. Positive values of s/c correspond to the suction surface of the airfoil.

and account for mass and heat fluxes of the runback ice were introduced into the model formulation proposed by Silva [18]. The IPS substratum was modelled as a unique layer with an equivalent thermal conductivity and a fixed thickness.

2.2 Baseline Design

The layout of the ETIPS was taken from the experimental work of Al-Khalil [1]. The geometry consisted of an extruded NACA0012 profile with a chord of 0.9144 m. The IPS comprised a set of 7 multilayered heaters fitted at the leading edge expanding spanwise. Due to a manufacturing issue, the heaters have been shifted towards the suction side a total of 0.0145 m. Therefore, the geometry, depicted in Fig. 3, is not symmetric. The freestream velocity is equal to 89.4 ms^{-1} , the pressure is equal to 90 000 Pa, the angle of attack equal to 0° and the Static Air Temperature is equal to 251.33 K. As for the cloud properties the LWC is equal to $5.5e-4 \text{ kgm}^{-3}$ and the MVD is equal to $20 \text{ }\mu\text{m}$.

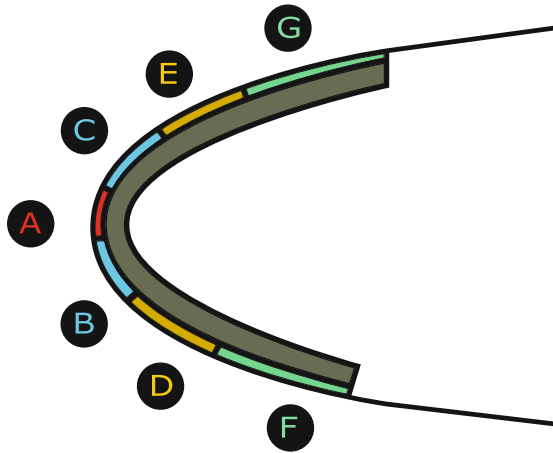


Fig. 3. Layout of the heaters of the ETIPS. Note that due to a manufacturing issue the heaters are shifted towards the CEG side

This layout and operation conditions were selected as the baseline test case for optimization because they represented a realistic problem for which actual improvements entailed by the optimization study would be quantified. The model validation results are shown in Fig. 4, where they are compared to experimental measurements reported in the work of Al-Khalil [1]. Computational results are in good agreement with experiments, in particular in the region of impingement. Due to fixed cloud and flight parameters, the mass impinging is computed only once through the Aerodynamic and Particle Tracking solvers. Therefore, each model evaluation included only the solution to the thermodynamic model. This rendered the computational cost per evaluation in the order of 20 s. The simulations were run in a single node from a cluster, which included two Intel Xeon

X5650 processors with a base frequency of 2.67 GHz. Each consists of 6 cores with 2 threads each, 24 threads in total.

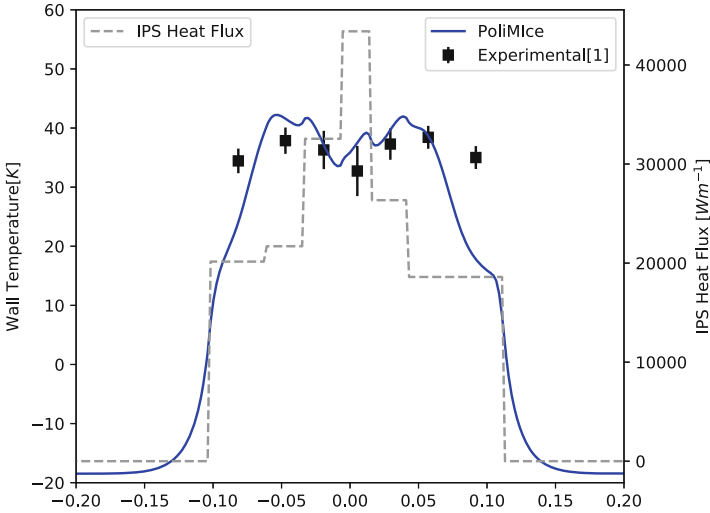


Fig. 4. Comparison of the experimental surface temperature readings from the work of Al-Khalil [1] and the predictions from the ETIPS numerical model

3 Optimization Methodology

3.1 Problem Formulation

The target of the optimization is the minimization of the thermal power consumption of the ETIPS constrained to no-runback ice formations downstream the protected parts. The designs for which the freezing mass rate was greater than $1e-7 \text{ kgs}^{-1}$ were considered infeasible. The design vector \mathbf{P} included the heat fluxes corresponding to each heater. A linear penalty method was chosen to handle the constraint. The amount of constraint violation was integrated into the objective function as a penalty. The penalty was chosen to be linearly proportional to the amount of extra-power that would be required to evaporate the freezing mass rate. Hence, the formulation of the optimization problem for a discrete domain reads:

$$\underset{\mathbf{P} \in \mathbb{R}^7}{\text{minimize}} \quad \sum_{i=1}^7 P_i \Delta l_i + k \sum_{i=1}^N \dot{m}_{ice}(s_i) i_{l-v} \tag{4a}$$

$$\text{subject to} \quad P_i \geq 0 \text{Wm}^{-2} \tag{4b}$$

$$P_i \leq 45\,000 \text{Wm}^{-2}, \tag{4c}$$

where k is an integer proportionality factor. Low k values drove the optimization algorithm to the infeasible region of the design space. High values stopped the

exploration of the portions of the design space close to the constraint. Two different values were tested namely, $k = 3$ and $k = 10$. When the constraint was inactive, the objective function solely depended linearly on the heat fluxes. Further decrease of the heat fluxes lead to the formation of runback ice, activating the constraint. At that point, the monotony of the objective function changed due to the penalty. Consequently, the global minimum must lay at the feasibility boundary.

3.2 Optimization Algorithm Description

GAs were selected as the preferred optimization algorithm because the objective function included nonlinearities and multiple local minima. These features were associated with the inclusion of the penalty, which also introduced noise to the objective function. That was due to the coupling of several numerical models with their associated numerical errors. For these reasons, gradient-based algorithms could misperform here. In addition, GAs are easily scaled to multi-objective problems, allowing future problem exploitation. Finally, GAs are simple, mature, widely proven and versatile algorithms that have successfully optimized complex objective functions with different features when adequate parameters are set [4]. Their main drawback is the slow or no convergence to the exact global minimum and the requirement of parameter tuning. The computational cost per evaluation of the ETIPS numerical model is low, enabling numerous repeated samples.

GAs are inspired by the survival of the fittest individuals in a population. Each individual is represented by a chromosome containing the input parameters and by its fitness that accounts for its respective objective function value. The input parameters were encoded forming a binary string, the chromosome in which each bit mimics a gen. Bit encoding can perform equally well than real value encoding as reported by De Jong [5]. Among its benefits are the ease of performing the operations of Crossover and Mutation. A total of 23 bits per design variable were required to get an accuracy of 0.01. The selected generic operators for the evolution of the population were Roulette Selection, One-point Crossover, Bit-flip Mutation and Elitism for the single best individual of a population [11]. The selection of operator parameters and population size is of paramount importance for the adequate performance of the algorithm. In this work, they were extracted from the parameter study performed by Deb for a multiple peak function [6]. Selection operator performs the exploitation of local portions of the design space to find a minimum. Crossover and Mutation operators account for two different paradigms for exploration and exploitation. To investigate the suitability of each, their performance was investigated in Crossover-based GA (C-GA) and Mutation-based GA (M-GA) as well as combined (CM-GA). A constant population of 500 individuals was selected. In a preliminary study, a population of 100 individuals presented premature convergence as well as poor population diversity for C-GA, M-GA and CM-GA, Operators parameters p_{cr} and p_m were set to 0.9 and $\frac{1}{7}$ respectively as suggested by Deb [6]. The stopping criterion was set to 100 000 function evaluations per run. To cope with the characteristic randomness of the algorithm, each of the runs was repeated 5 times.

4 Results

A summary of results is depicted in Table 1, where the best objective function values H_b for each GA and k are reported with their respective constraint values \dot{m}_{ice} and the arithmetic mean of the minimized power consumption of all the 5 runs H_A .

Table 1. Best and Average Performance of the 5 runs for each of the GA tested and different penalty factors. The values reported account only for the power consumption, not including constraint violation penalties.

k	C-GA			M-GA			CM-GA		
	H_b	\dot{m}_{ice}	H_A	H_b	\dot{m}_{ice}	H_A	H_b	\dot{m}_{ice}	H_A
3	4 249	1.48e-6	4 289	4 329	2.75e-6	4 369	4 293	5.98e-7	4 342
10	4 286	0.00	4 341	4 249	0.00	4 287	4 328	0.00	4 381

First, it was observed that for $k = 10$, the optimized solutions for each run were generally feasible. Hence, the exploration of the design space focused the search in the feasible and linear portion of the design space. The best performing GA on average and individually was M-GA for the parameters selected. It retrieved the overall best optimized solution, which decreased the thermal power consumption by 11.8%, pushing the design to the feasible space. Besides, it presented the minimal difference between H_A and H_b showing better consistence. Nevertheless, CM-GA was the poorest performing algorithm caused by an excess of exploration or sub-optimal parameter selection that slowed the convergence. On the other hand, for $k = 3$, penalties were small enough such that infeasible solutions were well-performing. As stated in Sect. 3, the landscape of the infeasible region is more complex. Because of that, more exploration was needed making C-GA and CM-GA more adequate choices for the parameters selected. The best performing GA was C-GA for both H_b and H_A . The Mutation operator performed exploration and exploitation actions even in a heterogeneous population whereas the Crossover operator conducted exploitation only for homogeneous populations. The selected large population and random Selection operator maintained diversity in the population. However, in the feasible space, further exploitation given by M-GA was suitable and thorougher exploration performed by CM-GA ill-performed.

The convergence histories for the 5 runs of M-GA and $k = 10$ are depicted in Fig. 5. Analogous results were found for the remaining GAs and runs. The computational cost per run was in the range of $2e5$ s. One can see that the convergence rate was slow, not reaching it clearly in any of the runs. Besides, each run converged to a different value. This was due to the presence of several local minima, inherent inefficiency of the GA or sub-optimal parameter selection. Furthermore, the selective pressure was low. That was caused by the population size and the uniform Selection operator that maintained alive unfit individuals

and their genetic information by chance. On a different note, any minimum must lie at the feasible boundary, dictated by the ice formation threshold. Otherwise, H_b could be further reduced manually by decreasing any P_i until reaching it. Consequently, in these runs no minimum was reached.

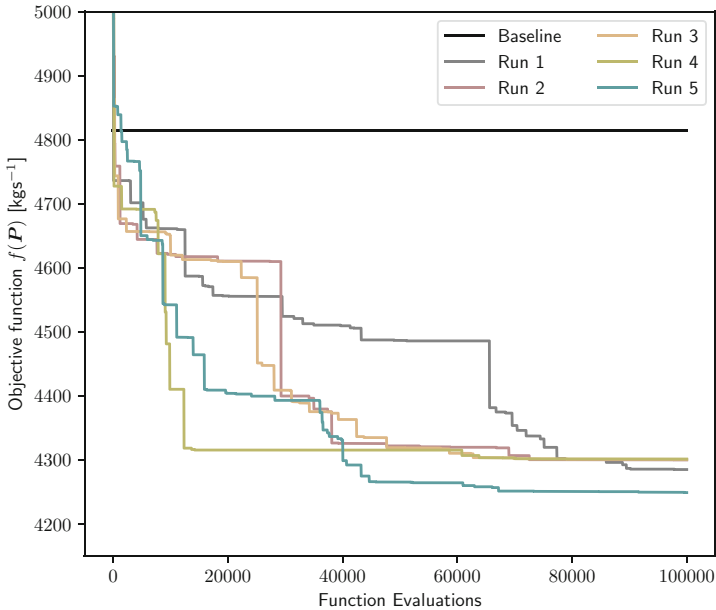


Fig. 5. Convergence history over the course of the simulations. Convergence was still not reached.

Next, the results obtained for the optimized design are presented in Fig. 6 and Table 2. It was found that the optimal design minimized as well the convective losses. In the baseline design, those accounted for 38% of the total thermal power and 31% in the optimized design. That was achieved by shortening the liquid film and nearly turning off heaters F and G. All the excess heat supplied to them would be dissipated by the air. At stagnation point, there is a prominent temperature drop. Large portion of heat is taken there to warm impinging droplets. Besides convective losses relative to the thermal power supply are maximum, hence keeping the heat flux low improved system performance. At the locations corresponding to heaters B, C, D and E, the relative convective losses were reduced. By raising the temperature there, the evaporation process was more efficient the mass evaporated increases exponentially with water temperature and convective losses depend linearly. In that way, a bigger portion of the thermal power supplied was devoted to evaporation, improving the efficiency of the ETIPS.

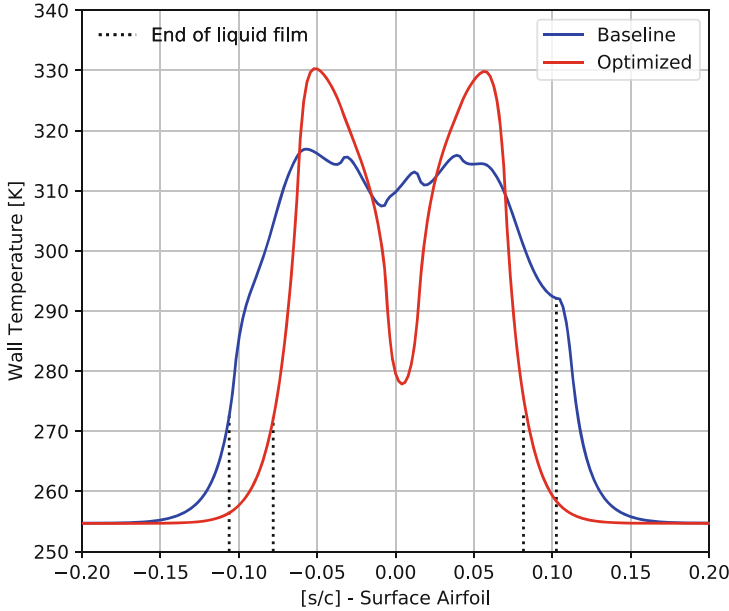


Fig. 6. Temperature predictions on the solid surface for baseline and optimized designs. Included additionally, the limits of the liquid film in each case for comparison

Table 2. Comparison of the heat fluxes and total power consumption per meter span protected for baseline and optimized designs.

Heat flux [Wm ⁻²]	Heater A	Heater B	Heater C	Heater D	Heater E	Heater F	Heater G	Power [Wm ⁻¹]
Base	43 400	32 550	26 350	21 700	18 600	20 150	18 600	4 815
Opt	6 328	39 378	39 476	41 853	43 039	0	239	4 250

5 Final Remarks

Any of the GA alternatives was successful in finding the designs that outperformed the initial intuitive design within few function evaluations. However, convergence to a minimum was slow and frequently non reached. In addition, the global minimum was not identified either. This evidenced the shortcomings of GA under sub-optimal parameters selection. Nevertheless, it was concluded that deploying a more aggressive elitist strategy could speed up convergence. For instance, elitist parent-off spring survival to fill the population size, which provided promising results in preliminary runs. Moreover, the number of bits chosen for the binary encoding of each of the variables should be investigated as well for improved convergence. With regards to the allocation of heat fluxes, it was found that an optimal design presents minimal convective losses for the same amount of evaporative heat fluxes. This could be achieved by increasing the

water temperature in locations of relatively low convective losses and shrinking the liquid film. Furthermore, the heat fluxes in dry parts should be low or otherwise, the convective losses would rapidly escalate. Due to the accuracy of the numerical model presented in Sect. 2, a mismatch is expected between the best solution here presented and reality. However, the qualitative design guidance can be helpful on the allocation of heat fluxes on the heaters of an ETIPS.

Acknowledgements. The work in this paper was supported by the H2020-MSCA-ITN-2016 UTOPIAE, grant agreement 722734.

References

1. Al-Khalil, K.M., Horvath, C., Miller, D.R., Wright, W.B.: Validation of NASA thermal ice protection computer codes. Part 3; The validation of ANTICE. In: 35th Aerospace Sciences Meeting and Exhibit, p. 51 (2001)
2. Beaugendre, H., Morency, F., Habashi, W.G.: FENSAP-ice's three-dimensional in-flight ice accretion module: ICE3D. *J. Aircr.* **40**(2), 239–247 (2003)
3. Bellosta, T., Parma, G., Guardone, A.: A robust 3D particle tracking solver of in-flight ice accretion using, arbitrary precision arithmetics. In: VIII International Conference on Coupled Problems in Science and Engineering (2019)
4. Cavazzuti, M.: *Optimization Methods: From Theory to Design Scientific and Technological Aspects in Mechanics* (2012)
5. De Jong, K.: *Evolutionary Computation: A Unified Approach*. MIT Press, Cambridge (2006)
6. Deb, K., Agrawal, S.: Understanding interactions among genetic algorithm parameters. In: *Foundations of Genetic Algorithms*, pp. 265–286 (1998)
7. Dussin, D., Fossati, M., Guardone, A., Vigeveno, L.: Hybrid grid generation for two-dimensional high-Reynolds flows. *Comput. Fluids* **38**(10), 1863–1875 (2009)
8. Economon, T.D., Palacios, F., Copeland, S.R., Lukaczyk, T.W., Alonso, J.J.: SU2: an open-source suite for multiphysics simulation and design. *AIAA J.* **54**(3), 828–846 (2016)
9. Gent, R., Dart, N., Cansdale, J.: Aircraft icing. *Philos. Trans. Roy. Soc. Lond. Ser. A Math. Phys. Eng. Sci.* **358**(1776), 2873–2911 (2000)
10. Lynch, F.T., Khodadoust, A.: Effects of ice accretions on aircraft aerodynamics. *Prog. Aerosp. Sci.* **37**(8), 669–767 (2001)
11. Michalewicz, Z.: *Genetic Algorithms + Data Structures = Evolution Programs*. Springer, Heidelberg (2013)
12. Myers, T., Charpin, J., Chapman, S.: Modelling the flow and solidification of a thin liquid film on a three-dimensional surface. In: Di Bucchianico, A., Matthéij, R., Peletier, M. (eds.) *Progress in Industrial Mathematics at ECMI 2004*, pp. 508–512. Springer, Heidelberg (2006). <https://doi.org/10.1007/3-540-28073-1-76>
13. Pellissier, M., Habashi, W., Pueyo, A.: Optimization via FENSAP-ICE of aircraft hot-air anti-icing systems. *J. Aircr.* **48**(1), 265–276 (2011)
14. Petty, K.R., Floyd, C.D.: A statistical review of aviation airframe icing accidents in the US. In: *Proceedings of the 11th Conference on Aviation, Range, and Aerospace Hyannis*, pp. 623–628 (2004)
15. Politovich, M.: Aircraft icing. In: *Encyclopedia of Atmospheric Sciences*, vol. 358, no. 1776, pp. 68–75 (2003)

16. Pourbagian, M., Habashi, W.G.: Surrogate-based optimization of electrothermal wing anti-icing systems. *J. Aircr.* **50**(5), 1555–1563 (2013)
17. Pourbagian, M., Talgorn, B., Habashi, W.G., Kokkolaras, M., Le Digabel, S.: Constrained problem formulations for power optimization of aircraft electro-thermal anti-icing systems. *Optim. Eng.* **16**(4), 663–693 (2015)
18. Silva, G., Silvaes, O., de Jesus Zerbini, E.: Numerical simulation of airfoil thermal anti-ice operation, Part 1: Mathematical modelling. *J. Aircr.* **44**(2), 627–633 (2007)
19. Silva, G., Silvaes, O., Zerbini, E., Hefazi, H., Chen, H.H., Kaups, K.: Differential boundary-layer analysis and runback water flow model applied to flow around airfoils with thermal anti-ice. In: 1st AIAA Atmospheric and Space Environments Conference, p. 3967 (2009)